Ukrainian Journal of Physical Optics
ISSUE 3
2024

SPECTROSCOPIC AND OPTICAL-LUMINESCENT PROPERTIES OF THE $Li_2B_4O_7$:Mn, Er GLASS

B.V. PADLYAK[1,2], I.I. KINDRAT[2], A. DRZEWIECKI[2], V.T. ADAMIV[1]

[1] Vlokh Institute of Physical Optics of the Ivan Franko National University of Lviv, 23 Dragomanov Str., 79005 Lviv, Ukraine
[2] University of Zielona Góra, Institute of Physics, Division of the Spectroscopy of Functional Materials, 4a Szafrana Str., 65-516 Zielona Góra, Poland

Received: 14.05.2024

Abstract. High-quality $Li_2B_4O_7$:Mn, Er glass samples containing 1.0 mol.% of MnO_2 and Er_2O_3 were obtained firstly by melt-quenching technology and studied by X-ray diffraction (XRD), electron paramagnetic resonance (EPR) and optical-luminescent methods. Local structure parameters (interatomic distances and coordination numbers) of the $Li_2B_4O_7$:Mn, Er glass were derived from the radial distribution function calculated from the experimental XRD curve. Analysis of EPR and optical spectroscopy (absorption, luminescence excitation, emission, decay kinetics) data shows the presence of $Mn^{2+}(3d^5)$, $Mn^{3+}(3d^4)$, and Er^{3+} $(4f^{11})$ ions in the $Li_2B_4O_7$:Mn, Er glass network. Particularly, in the studied glass have been identified three types of Mn^{2+} centers: single Mn^{2+} (1) ions in the strongly distorted sites of rhombic symmetry (ratio of rhombic and axial constants $|E/D| \leq 1/3$), single Mn^{2+} (2) ions in sites of almost cubic symmetry ($D \cong 0$, $E \cong 0$), and Mn^{2+} pairs and small clusters, coupled by magnetic dipolar and exchange interactions. The optical absorption spectrum of the $Li_2B_4O_7$:Mn, Er glass shows a very broad, intense band peaked at 467 nm that belongs to the $^5E_g(D) \rightarrow {}^5T_{2g}(D)$ transition of Mn^{3+} ions and a number of weak narrow lines belonging to $f - f$ transitions of the Er^{3+} $(4f^{11}, {}^4I_{15/2})$ ions. The emission spectrum of the $Li_2B_4O_7$:Mn, Er glass exhibits a broadband corresponding to the $^4T_{1g}(G) \rightarrow {}^6A_{1g}(S)$ transition of Mn^{2+} ions. Luminescence spectra and decay kinetics of Mn^{2+} centers in the $Li_2B_4O_7$:Mn, Er glass were discussed and compared with corresponding results for $Li_2B_4O_7$:Mn glass. The absence of characteristic Er^{3+} and Mn^{3+} photoluminescence in the $Li_2B_4O_7$:Mn, Er glass is clarified by proposed energy transfer mechanisms from Er^{3+} to Mn^{2+} and Mn^{3+} ions.

Keywords: $Li_2B_4O_7$:Mn, Er glass, XRD, EPR, optical absorption, photoluminescence, decay kinetics, energy transfer
UDC: 535.37
DOI: 10.3116/16091833/Ukr.J.Phys.Opt.2024. 03105

1. Introduction

Glasses and crystals doped with rare-earth elements show good optical characteristics and high luminescence efficiency, making them applicable for solid-state lighting, laser technology, and other useful applications in modern technics [1,2]. The erbium (Er) impurity belongs to the rare-earths group and can exist as Er^{3+} $(4f^{11}, {}^4I_{15/2})$ and/or Er^{2+} $(4f^{12}, {}^3H_6)$ ions in various glassy and crystalline materials. The Er^{3+} ions are very important for developing of lasers, optical amplifiers, and fiber optic communication systems [3–6].

This also concerns the Er^{3+}-doped borate glasses. The Er^{3+}-doped borate glasses are better than corresponding borate crystals in applications where ease of fabrication and flexibility in shape and size are crucial. In particular, Er^{3+}-doped borate glasses can be incorporated into the core of optical fibers. Besides this, the Er^{3+}-doped borate glasses can also be used as easily fabricated gain media in solid-state lasers, including IR lasers. Researchers are continue studying of the Er^{3+}-doped borate glasses for better performance in laser technique and other applications.

Many research articles [7–13] on optical spectroscopy and luminescence of the Er^{3+}-doped borate glasses have been published to the present. In these articles, the emission and excitation spectra and the luminescence decay kinetics of the Er^{3+} ions were investigated and discussed. Some published articles [10,11] focused on the preparation technology and studies of the structure and physical properties of the borate glasses. It is attempted to optimize the basic glass composition to improve the Er^{3+} luminescence properties in the Er-doped borate glasses.

Our research group has reported studies on Er-doped $Li_2B_4O_7$ ($Li_2O–2B_2O_3$) glasses in [7,12]. The $Li_2B_4O_7$:Er glasses containing 0.5 and 1.0 mol.% of Er_2O_3 were studied in detail by EPR, optical absorption, and luminescence (excitation, emission spectra, decay kinetics) spectroscopy as well as Judd–Ofelt theory in [7]. Later, spectroscopic properties of the $Li_2B_4O_7$:Er glass containing 1.0 mol.% of Er_2O_3 and the $Li_2B_4O_7$:Er, Ag glass containing 1.0 and 2.0 mol.% of Er_2O_3 and $AgNO_3$ were studied and compared to each other in [12]. Emission spectra of the $Li_2B_4O_7$:Er and $Li_2B_4O_7$:Er, Ag glasses show strong infrared and green emission bands peaked at 1530 nm and 546 nm, respectively. These bands are related to the $^4I_{13/2} \rightarrow {}^4I_{15/2}$ and $^4S_{3/2} \rightarrow {}^4I_{15/2}$ transitions of Er^{3+} ions. Enhancement of the green emission band in the $Li_2B_4O_7$:Er, Ag glasses was reported in [12] that was explained by $Ag^+ \rightarrow Er^{3+}$ energy transfer and local field effects caused by surface plasmon resonance (SPR) of the Ag metallic nanoparticles. Thus, co-doping of the $Li_2B_4O_7$:Er glass with other chemical elements may be useful for increasing of the Er^{3+} emission efficiency in both the green and IR spectral ranges.

Manganese (Mn) is a transition metal ($3d^54s^2$ electron configuration) that can exhibit different valence states in oxide compounds. The most common and stable valence (oxidation) states of Mn as an impurity in oxide compounds are Mn^{2+} ($3d^5$ electron configuration), Mn^{3+} ($3d^4$), and Mn^{4+} ($3d^3$). Particularly, in Mn-doped oxide glasses, the coexistence of Mn^{2+} and Mn^{3+} ions is usually observed [13–15]. The Mn^{2+} ions can be detected by EPR and luminescence spectroscopy methods, whereas the Mn^{3+} ions can be detected by optical absorption [13–15]. This is possible because the Mn^{2+} ions exhibit characteristic EPR and luminescence (emission and excitation) spectra, whereas the Mn^{3+} ions exhibit a broad characteristic absorption band [13–15]. Thus, EPR and optical (absorption and luminescence) spectroscopy are two important techniques for studying the electronic structure and properties of manganese ions in different compounds.

The effect of Mn co-doping of the Er^{3+}-doped materials can reveal several essential effects on their optical and luminescent properties. Co-doping with Mn impurity together with Er^{3+} ions can enhance their luminescence intensity due to energy transfer. In addition, it may be possible to tune the emission properties of the Mn and Er co-doped materials over a wide spectral range.

Until now, there have not been many detailed studies in the literature on materials co-doped with Mn and Er. Let us briefly review some of the available articles. The photoluminescence emission and excitation spectra of Er and Mn co-doped chalcogenide glass with the composition $As_{12}Ge_{33}Se_{55}$ were studied in [16]. Mn was found to decrease the intensity of the Er^{3+} emission in the NIR spectral range [16]. The structure and optical properties of Er and Mn co-doped $SrAl_2O_4$ phosphor were investigated in [17]. As a result of the energy transfer from Mn^{2+} to Er^{3+} ions, the Er^{3+} emission band at 1530 nm is enhanced [17]. The far-red and green emission of Mn^{4+} and Er^{3+} ions, respectively, was registered in the La_2ZnTiO_6:Mn^{4+}/Er^{3+}

phosphor under excitation at 379 nm [18]. A very efficient $Er^{3+} \rightarrow Mn^{4+}$ energy transfer was observed in [18]. Dual emission from both Er^{3+} (peaks at 531, 545, and 677 nm) and Mn^{2+} (peak at 610 nm) activators was observed in the CaZnOS:Er/Mn crystal [19]. Recently, the $CsPbCl_3:Mn^{2+}$, Er^{3+} quantum dots were studied in [20]. In this work, the strong and intense luminescence peak around 600 nm, ascribed to Mn^{2+} ions, was observed. Photoluminescence of Er^{3+} ions was not observed, but the incorporation of Er^{3+} enhances the emission of Mn^{2+} ions. It should be noted that the highest quantum yield of Mn^{2+} luminescence in the $CsPbCl_3:Mn^{2+}$, Er^{3+} quantum dots was obtained at a Mn:Er ratio of 1:1.

It can be seen from the above review that the character and efficiency of the energy transfer cannot be predicted as a priory. In some materials, energy transfer from Mn to Er is observed with the quenching of Mn emission and enhancement of Er emission. In other materials, quenching of Er emission and enhancement of Mn emission is observed due to energy transfer from Er to Mn. Each case of co-doping in each material requires its own study. From the analysis of referenced data on Er and Mn co-doping, it can also be seen that the influence of Mn impurity on the spectroscopic properties of Er^{3+} ions in borate glasses has not been investigated in detail up to now.

Therefore, this work aims to investigate the effect of simultaneous Mn and Er co-activation on spectroscopic and optical-luminescent properties of the $Li_2B_4O_7$ glass. The main aim of the article is to investigate changes in the local structure, spectroscopic, and photoluminescent properties of the $Li_2B_4O_7$ glass caused by co-doping with Mn and Er impurities.

2. Experimental details

2.1. Synthesis of the $Li_2B_4O_7$:Mn, Er glass and samples preparation

The $Li_2B_4O_7$:Mn, Er glass was obtained by the standard melt-quenching technology of borate glasses represented in [7,12,21,22]. For obtaining the $Li_2B_4O_7$ glass, the Li_2CO_3 compound and the boric acid (H_3BO_3) were used. The Mn and Er impurities were added to the raw materials as MnO_2 and Er_2O_3 oxides, respectively, in amounts of 1.0 mol.%. The raw materials in the stoichiometric proportion were thoroughly mixed, placed into a corundum ceramic crucible and then its was put in a furnace for the melting process. The entire process of the studied glass preparation was realized in the air. The Mn-Er co-doped $Li_2B_4O_7$ glass was made by rapid cooling of the melt. The technological process for obtaining the $Li_2B_4O_7$:Mn, Er glass can be presented by the following multi-step chemical reaction:

$$\begin{gathered} Li_2CO_3+4H_3BO_3+MnO_2+Er_2O_3 \xrightarrow[170^oC]{4H_2O\uparrow} Li_2CO_3+4(\alpha\text{-}HBO_2)+MnO_2+Er_2O_3 \xrightarrow[250^oC]{2H_2O\uparrow} \\ Li_2CO_3+2B_2O_3+MnO_2+Er_2O_3 \xrightarrow[800^oC]{CO_2\uparrow} Li_2B_4O_7+MnO_2+Er_2O_3 \xrightarrow[\sim 1000^oC]{\text{melting}} \\ Li_2B_4O_7:Mn,Er\ \text{melt} \xrightarrow[\text{cooling}]{\text{rapid}} Li_2B_4O_7:Mn,Er\ \text{glass} \end{gathered} \quad (1)$$

From the obtained $Li_2B_4O_7$:Mn, Er glasses were prepared samples for optical absorption and photoluminescence (emission, excitation, and decay kinetics) studies by cutting and polishing them to a size of $12\times8\times2$ mm^3. The $Li_2B_4O_7$:Mn, Er glass samples with an approximate size of $3\times2\times2$ mm^3 were used for investigations by XRD and EPR techniques.

2.2. Experimental methods and equipment

The XRD pattern was registered using a computerized DRON-3 X-ray diffractometer with Cu Kα radiation (λ=1.5418 Å). The paramagnetic centers in the $Li_2B_4O_7$:Mn, Er glass were

investigated using a multifrequency and multi-resonance FT-EPR spectrometer Bruker (model Elexsys E 580 – 10/12) operating in the X-band (work frequency ν=9.851013 GHz) at room temperature (T=295 K) and in the 6.7 – 100 K temperature range using a helium flow cryostat.

Optical absorption spectra were recorded at room temperature (T=295 K) using the UV-2600 Shimadzu spectrophotometer equipped with the ISR-2600Plus two-detector integrating sphere attachment. The spectrophotometer includes a double-beam photometric system, halogen and deuterium lamps, and a single diffraction grating. The measurement range of the UV-2600 Shimadzu spectrophotometer with ISR-2600Plus attachment is 220 – 1400 nm. The photoluminescence emission and excitation spectra and emission decay curves were recorded at T=295 K using a FluoroMax–4P Horiba spectrofluorimeter. The spectrofluorimeter is equipped with a 150 W xenon lamp, two grating monochromators (one for excitation and one for emission), and the R928P photomultiplier tube.

3. Results and discussion

3.1. The XRD investigation of the $Li_2B_4O_7$:Mn, Er glass

The experimental XRD data for the $Li_2B_4O_7$:Mn, Er sample, plotted as a function of 2θ scattering angle, are given by circles in Fig. 1. The smoothed XRD pattern without narrow crystalline peaks presented by the red curve in Fig. 1 confirms the disordered structure of the studied sample.

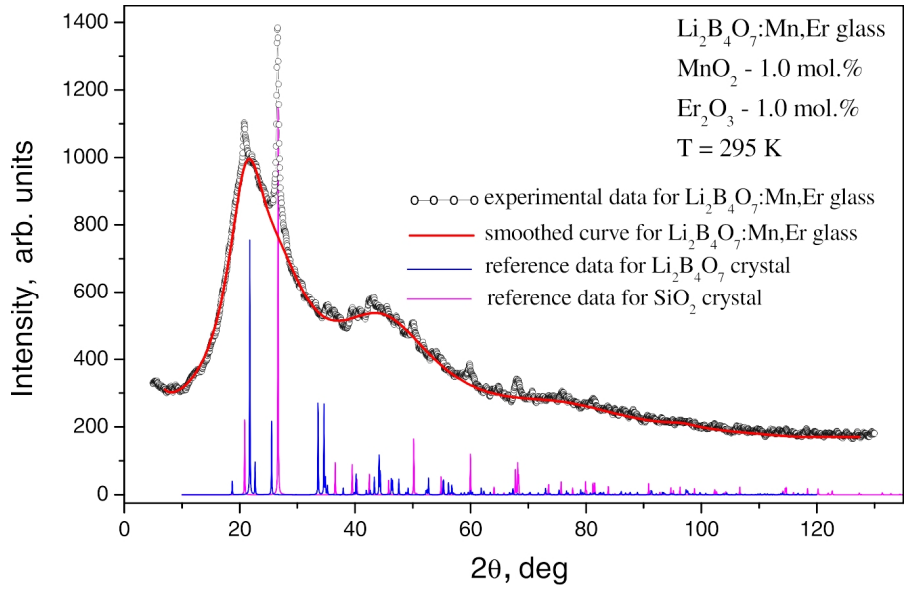

Fig. 1. The experimental XRD data (circles) and smoothed XRD curve (red line) for studied $Li_2B_4O_7$:Mn, Er glass as well as reference data for $Li_2B_4O_7$ crystal (blue line) [23] and SiO_2 crystal (magenta line) [24], plotted as functions of 2θ scattering angle. The numbers of XRD standard cards for $Li_2B_4O_7$ (ICDD 18-0717) and SiO_2 (ICDD 46-1045) crystals.

Relatively narrow peaks near 21° and 27° in the experimental XRD profile correspond to the impurity of SiO_2 polycrystalline compound (see magenta line in Fig. 1 [24] and XRD standard card ICDD 46-1045 for SiO_2 crystal). It should be noted that for all borate glasses obtained by us in corundum crucibles, the SiO_2 impurity is typical, and its concentration

depends on the temperature of the melt. In our opinion, the presence of the SiO_2 impurity in the obtained glass is caused by Si diffusion from the crucible. It is noteworthy that the main maxima in the XRD profile of the $Li_2B_4O_7$:Mn, Er glass are close to the positions and intensities of the main reference peaks for the $Li_2B_4O_7$ crystal (see blue line in Fig. 1 [23] and XRD standard card ICDD 18-0717 for $Li_2B_4O_7$ crystal).

The registered XRD curve was analyzed to learn the local structure of the $Li_2B_4O_7$:Mn, Er glass, including interatomic distances and coordination numbers. The intensity of scattered radiation, $I(s)$, of a system of atoms, can be written as follows:

$$I(s) = NF^2(s)\left\{1 + \int_0^{\infty} 4\pi r^2 [\rho(r) - \rho_0] \frac{\sin sr}{sr} ds\right\}, \quad (2)$$

where $s = 4\pi \sin\theta/\lambda$ is the modulus of the scattering vector, λ = 1.5418 Å, N is the number of atoms, $F^2(s)$ is the atomic structure factor, r is the distance, $\rho(r)$ is the atomic density, ρ_0 is the average atomic density. Using the Fourier transformation of Eq. (2) was obtained the radial distribution function (RDF) in the following form:

$$4\pi r^2 \rho(r) = 4\pi r^2 \rho_0 + \frac{2r}{\pi} \cdot \int_{s_1}^{s_2} s\left[\frac{I(s)}{NF^2(s)} - 1\right] \sin(sr) ds\,. \quad (3)$$

Radial distribution function $4\pi r^2\rho(r)$ describes the variation of the atomic density in dependence of r.

Fig. 2 shows the radial distribution function and its deconvolution into partial radial distribution functions. It highlights the average interatomic distances for specific atom pairs within different coordination spheres of the $Li_2B_4O_7$:Mn, Er glass. Table 1 gives the average distances between neighboring atoms and the number of atoms surrounding a given atom in the first coordination sphere of the $Li_2B_4O_7$:Mn, Er glass network. The coordination numbers for B and Li atoms in the $Li_2B_4O_7$:Mn, Er glass given in Table 1 were calculated by integrating the corresponding partial radial distribution functions (Fig. 2).

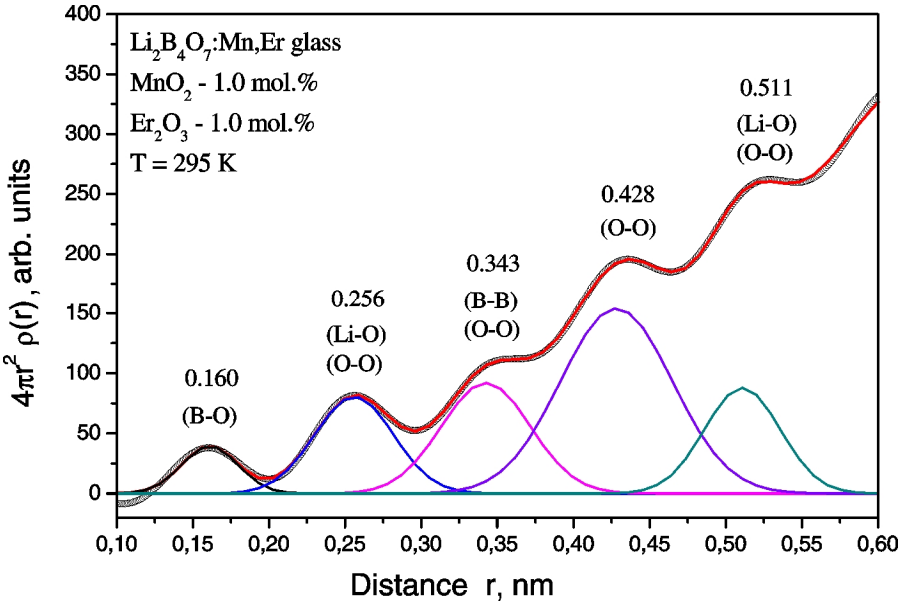

Fig. 2. Radial distribution function and its deconvolution into partial radial distribution functions, obtained for the $Li_2B_4O_7$:Mn, Er glass network.

Table 1 presents the corresponding average interatomic distances ($r_{B\text{-}O}$, $r_{Li\text{-}O}$) and coordination numbers ($N_{B\text{-}O}$, $N_{Li\text{-}O}$) in the network of $Li_2B_4O_7$:Mn, Sm [25], and $Li_2B_4O_7$ [22] glasses for comparison. Average interatomic distances for pairs in more distant coordination spheres are not analyzed due to the significant overlap of deconvoluted functions.

Based on the results obtained (see Fig. 2 and Table 1), it can be concluded that the BO_3 triangles and BO_4 tetrahedra are the main glass-forming units in the $Li_2B_4O_7$:Mn, Er glass network. The Li atoms are mainly the $Li_2B_4O_7$:Mn, Er glass network modifiers with the coordination number $N_{Li\text{-}O} \cong 4 - 7$. Obtained in this work structural results for $Li_2B_4O_7$:Mn, Er glass show satisfactory agreement with corresponding results for un-doped $Li_2B_4O_7$ glass [22] and crystal [23] as well as $Li_2B_4O_7$:Mn, Sm glass [25].

Table 1. Average B–O and Li–O distances and coordination numbers to oxygen for B and Li atoms in the studied $Li_2B_4O_7$:Mn, Er glass, which were calculated from the radial distribution function (Fig. 2). Uncertainties for average interatomic distances and coordination numbers are ± 0.003 nm and ± 0.3, respectively.

Glass composition	r_{B-O} , [nm]	N_{B-O}	r_{Li-O} ,[nm]	N_{Li-O}
$Li_2B_4O_7$:Mn, Er glass (this article)	0.160	3.0 4.0	0.256	4.8
$Li_2B_4O_7$:Mn, Sm glass [25]	0.161	3.0 4.0	0.255	4.9
$Li_2B_4O_7$ glass [22]	0.165	3.5	0.279	4.4

Note. Structural parameters (interatomic distances and coordination numbers) for glasses $Li_2B_4O_7$:Mn, Sm, and $Li_2B_4O_7$ are presented in Table 1 for comparison with relevant structural parameters of the studied $Li_2B_4O_7$:Mn, Er glass.

The obtained structural results show that the local structure of the studied $Li_2B_4O_7$:Mn, Er glass, un-doped $Li_2B_4O_7$ glass [22], $Li_2B_4O_7$ crystal [23], and $Li_2B_4O_7$:Mn, Sm glass [25] is closely similar. It should be noted that the BO_3 and BO_4 glass-forming units, as well as the LiO_n (n = 4 – 7) modifiers in glasses $Li_2B_4O_7$:Mn, Er, $Li_2B_4O_7$:Mn, Sm [25], and $Li_2B_4O_7$ [22] are more distorted and are characterized by considerably greater average distances between atoms than the corresponding precise distances in the lattice of $Li_2B_4O_7$ crystal [23].

3.2. The EPR spectra of the $Li_2B_4O_7$:Mn, Er glass and their analysis

In Fig. 3 are the X-band EPR spectra of the $Li_2B_4O_7$:Mn, Er glass, registered in wide (a) and narrow (b) magnetic field scan ranges at room temperature (T = 295 K). The EPR spectrum, registered in a wide magnetic field range, consists of a broad band, denoted as $Mn^{2+}(1)$, a sharp line, denoted as $Fe^{3+}(1)$, and an intense broadband, denoted as $Mn^{2+}(2)$ (see Fig. 3a). The EPR signals, denoted as $Mn^{2+}(1)$ and $Mn^{2+}(2)$ in Fig. 3, were observed in a number of oxide glasses with different basic compositions, doped with Mn and belonging to the Mn^{2+} ($^6S_{5/2}$, $3d^5$) ions [21,25–29]. The $Mn^{2+}(2)$ EPR signal containing six weakly-resolved hyperfine components related to the nuclei of ^{55}Mn isotope (natural abundance – 100%, nuclear spin I = 5/2) is best observed in a narrow magnetic field scan range (see Fig. 3b). Parameters of the Mn^{2+} EPR signals in the $Li_2B_4O_7$:Mn, Er glass have been determined at T = 295 K. For Mn^{2+} (1) centers were obtained the following parameters: isotropic g-factor g_{iso} = 4.29 ± 0.01 and peak-to-peak derivative linewidth ΔH_{pp} (1) ≅ 470 Gs with un-resolved hyperfine structure. For Mn^{2+} (2) centers were obtained the following parameters: isotropic

g-factor g_{iso} = 2.01 ± 0.01, peak-to-peak derivative linewidth ΔH_{pp} (2) ≅ 500 Gs with weakly-resolved six-component hyperfine structure, caused by nuclei of ^{55}Mn isotope, average value of the hyperfine interaction constant A_{av} = (89 ± 3) Gs and average peak-to-peak derivative linewidth of the hyperfine component ΔH_{pp}^{av} = (70 ± 3) Gs.

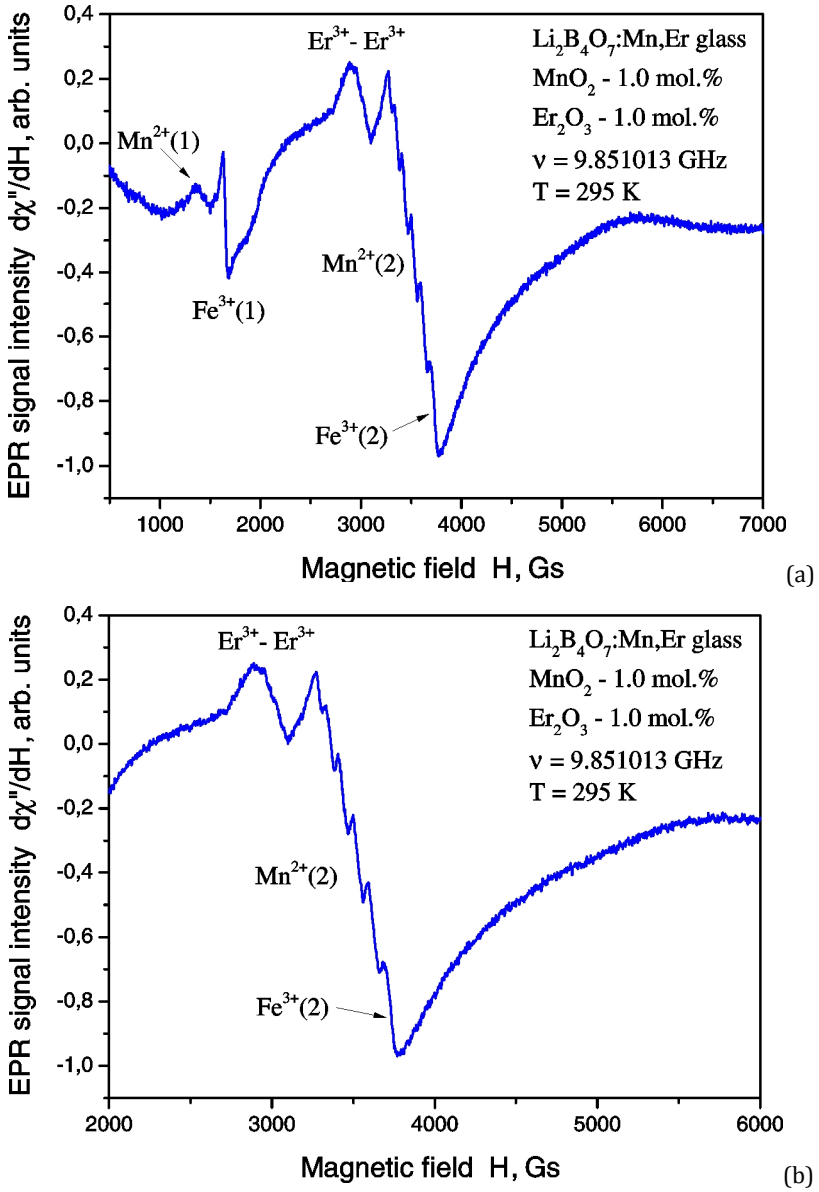

Fig. 3. The X-band EPR spectra of the $Li_2B_4O_7$:Mn, Er glass, registered at T = 295 K in wide (a) and narrow (b) ranges of the magnetic field.

Above is given the average value of the hyperfine interaction constant A_{av} = (89 ± 3) Gs for Mn^{2+} (2) centers, because the splitting between hyperfine components is significantly non-equidistant and equals about 71 Gs for the first and second components and about 109 Gs for the fifth and sixth components. The essential non-equidistance of the hyperfine components for Mn^{2+} (2) centers is caused by the influence of the zero-field splitting parameters D (axial crystal field term) and E (orthorhombic crystal field term), which leads to appearance of fine structure in the

EPR spectra of crystals. It is important to note that the local structure symmetry and zero-field splitting parameters (D and E) for $3d^5$-ions (Mn^{2+} and Fe^{3+}) in oxide glasses are a subject of controversial discussions in scientific literature up to now.

According to the interpretation given in [25–29], we can state that the isolated Mn^{2+} centers in the $Li_2B_4O_7$ glass network occupy strongly distorted sites of rhombic local symmetry, where ratio $|E/D| \leq 1/3$ that leads to the appearance of the Mn^{2+} (1) EPR signal with $g \cong 4.3$, and sites with a local symmetry close to cubic ($D \cong 0$, $E \cong 0$) that leads to the observation of the Mn^{2+} (2) EPR signal with $g \cong 2.0$. Various types of possible fully rhombic distortions (ratio $|E/D|=1/3$) of the octahedral and tetrahedral sites in glasses were discussed in [27]. The absence of hyperfine structure of the ^{55}Mn isotope nuclei for Mn^{2+} (1) centers is caused by a wide distribution of the zero-field splitting parameters (D and E) in the $Li_2B_4O_7$:Mn, Er glass network.

Besides the Mn^{2+} (1) and Mn^{2+} (2) EPR signals in the $Li_2B_4O_7$:Mn,Er glass is observed a broad (ΔH_{pp} more than 500 Gs) unresolved underlying response centered at $g \cong 2.0$ (see Fig. 3), which according to [21,25,26,28] is attributed to the Mn^{2+} – Mn^{2+} pair centers coupled by magnetic dipolar interaction. Thus, the Mn impurity is incorporated into the $Li_2B_4O_7$:Mn, Er glass network as isolated Mn^{2+} ions in the strongly distorted (Mn^{2+} (1) centres) and nearly cubic (Mn^{2+} (2) centers) octahedral or/and tetrahedral sites. Additionally, some parts of the Mn^{2+} impurity ions are revealed in the observed EPR spectrum as Mn^{2+} – Mn^{2+} pairs, coupled by magnetic dipolar interaction.

The Er impurity can become embedded into oxide compounds as paramagnetic Er^{3+} ($4f^{11}$, $^4I_{15/2}$) non-S-state Kramers ions and/or Er^{2+} ($4f^{12}$, $^3H_6$) non-paramagnetic ions. The Er^{3+} ions can be clearly identified by EPR and optical (absorption and luminescence) spectroscopy. According to [30], in zeolites, which are a class of disordered polycrystalline compounds, the non-S-state Kramers rare-earth ions (Ce^{3+}, Nd^{3+}, Dy^{3+}, and Yb^{3+}) show asymmetric EPR signals with an extremely broad line, which are observed at liquid helium temperatures only. The EPR spectra of Er^{3+} ions in disordered solids, including glasses, have been studied insufficiently up to now and published only in several articles [7,30–33]. In particular, the Er^{3+} asymmetric broad EPR signal with $g_{eff} \cong 9.78$ in the $Li_2B_4O_7$:Er and CaB_4O_7:Er glasses containing 0.5 and 1.0 mol.% Er_2O_3 for the first time was observed by us at 4 – 20 K [7]. Homogeneous broadening due to the shortening of spin-lattice relaxation time causes the Er^{3+} EPR signal to disappear at higher temperatures [7]. A similar broad EPR signal with a maximum near 80 mT (800 Gs) related to the Er^{3+} ions has also been observed in the Na_2O–GeO_2 glasses at liquid helium temperature [32].

For observation of the Er^{3+} ions, the X-band EPR spectra in the $Li_2B_4O_7$:Mn, Er glass were registered in the 6.7 – 100 K temperature range (Fig. 4). As one can see from Fig. 4, in the 6.7 – 20 K temperature range clearly is observed a new extremely broad asymmetric EPR signal with $g_{eff} \cong 9.78$ that is closely similar to the EPR signal observed at 4.2 – 20 K in $Li_2B_4O_7$:Er glasses activated with 0.5 and 1.0 mol.% of the Er_2O_3 impurity [7]. The observed EPR signal with $g_{eff} \cong 9.78$ (see Fig. 4) according to [7,30–33] belongs to the Er^{3+} single (isolated) centers in sites with strongly distorted octahedral geometry of the $Li_2B_4O_7$:Mn,Er glass network. This EPR signal of the Er^{3+} isolated centers disappears above T = 20 K (see Fig. 4 and Ref. [7]) as a result of shortening of the spin-lattice relaxation time. Therefore, the EPR spectroscopy at liquid helium temperatures clearly proves the presence of the Er^{3+} single

(isolated) centers in the studied $Li_2B_4O_7$:Mn, Er glass. On the basis of published data for Er^{3+} [7] it can be assumed that the EPR signal with $g_{eff} \cong 2.01$, observed in the $Li_2B_4O_7$:Mn, Er glass (see Fig. 3a, b) is related to the Er^{3+} – Er^{3+} pair centers, coupled by magnetic dipolar and exchange interactions. Therefore, the EPR spectroscopy shows the presence of Er^{3+} single centers as well as the Er^{3+} – Er^{3+} pair centers and their clusters in the studied $Li_2B_4O_7$:Mn, Er glass.

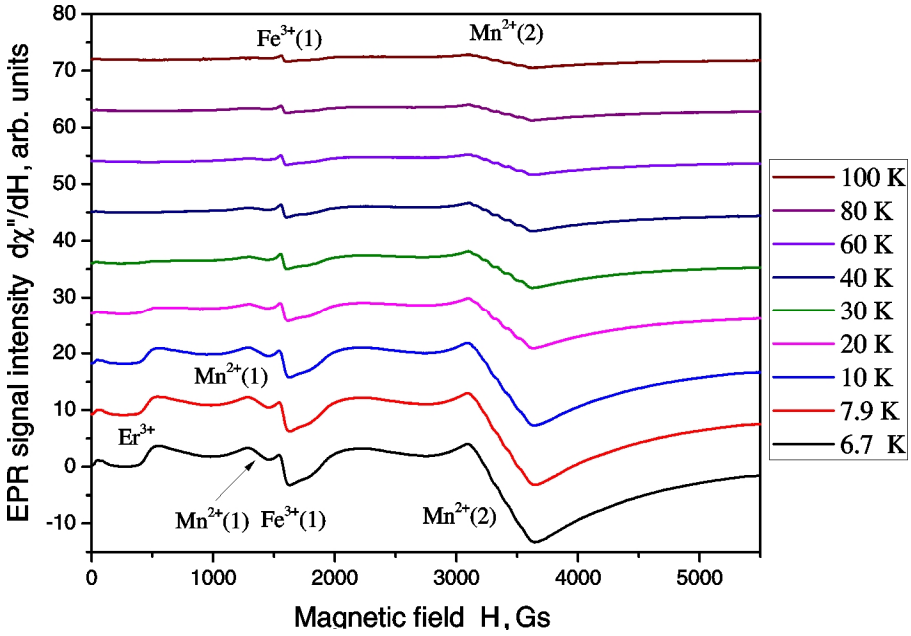

Fig. 4. The X-band EPR spectra of the $Li_2B_4O_7$:Mn, Er glass, registered in the range of 6.7 – 100 K.

It is worth noting that characteristic optical absorption and photoluminescence spectra of the non-paramagnetic Er^{2+} ($4f^{12}$, $^3H_6$) ions are not observed in the $Li_2B_4O_7$:Mn, Er glass (see *Subsections 3.3*, *3.4*, and *3.5*). Thus, according to EPR and optical spectroscopy data one can to conclude that the erbium impurity is incorporated into the $Li_2B_4O_7$ glass network exclusively as non-S-state Kramers Er^{3+} ($4f^{11}$, $^4I_{15/2}$) paramagnetic ions.

Additionally to the characteristic EPR signals of the Mn^{2+} and Er^{3+} ions, the $Li_2B_4O_7$:Mn, Er glass also shows single-line EPR signals with effective isotropic g-factors of $g_{iso} \cong 4.29$ and $g_{iso} \cong 2.00$, which are marked as $Fe^{3+}(1)$ and $Fe^{3+}(2)$ (see Fig. 3a, b and Fig. 4). These signals, according to [26–28], were ascribed to Fe^{3+} ($3d^5$, $^6S_{5/2}$) paramagnetic ions of the iron un-controlled impurity. The Fe^{3+} EPR signals observed in the $Li_2B_4O_7$:Mn,Er glass, are closely similar to the Fe^{3+} EPR signals, which previously have been observed by us and other authors in oxide glasses with different compositions [21,25–28,34–37]. The presence of the Fe^{3+} EPR signal with $g_{iso} \cong 4.29$ clearly indicates the disordered glassy structure of the studied $Li_2B_4O_7$:Mn, Er compound, which was also confirmed by the XRD data analysis described above. It should be noted that the concentration of the Fe^{3+} impurity ions in the $Li_2B_4O_7$:Mn, Er glass is relatively low. Therefore, very weak Fe^{3+} forbidden absorption bands cannot be seen in the optical absorption spectra, which are detailed and characterized below.

3.3. Optical absorption spectrum of the $Li_2B_4O_7$:Mn, Er glass

The optical absorption spectrum of the $Li_2B_4O_7$:Mn,Er glass, registered in the 250 – 1400 nm range, is presented in Fig. 5. The absorption spectrum with indicated transitions in the range

of 300 – 1350 nm is shown additionally as an inset in Fig. 5. A broad absorption band with a maximum in the blue spectral range and several narrow bands in the UV-Vis-IR range are observed. A strong increase in absorbance from 370 to 300 nm corresponds to band-to-band electronic transitions. The shift of absorption edge depending on structural features of borate crystals and glasses was discussed in [38]. It was found that the lowest in energy (highest in wavelength) band-to-band electronic transitions are associated with transitions from non-bridging oxygens to alkali cations. Therefore, transitions from non-bridging O^{2-} anions to Li^{+} cations may be responsible for the strong absorption from 370 to 300 nm in the $Li_2B_4O_7$:Mn, Er glass. A broad, intense asymmetric band that extends from 370 nm to 1000 nm reveals a maximum at 467 nm. This band belongs to the $^5E_g(D) \rightarrow {}^5T_{2g}(D)$ spin-allowed transition of Mn^{3+} ($3d^4$) ions in the high-spin configuration. The high-spin Mn^{3+} ions show a single absorption band only because the ^5D ground state term splits into two crystal field states ^5E_g and $^5T_{2g}$, and there are no other crystal field states with a multiplicity of 5.

.

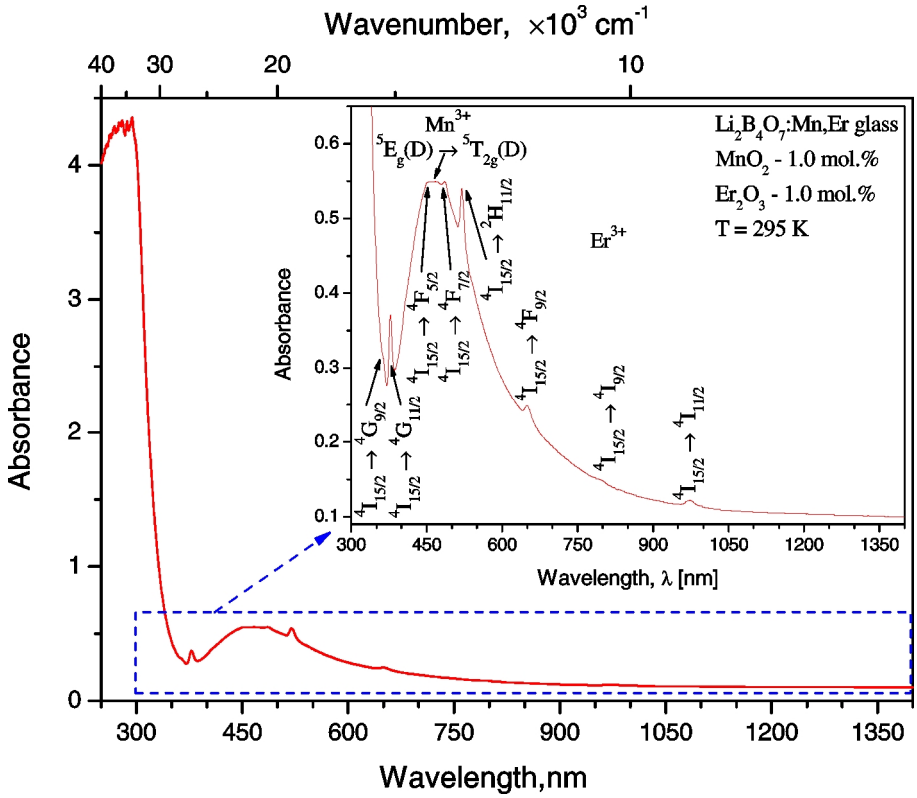

Fig. 5. Optical absorption spectrum of the $Li_2B_4O_7$:Mn, Er glass recorded at room temperature (T = 295 K).

Observed broad absorption band cannot originate from Mn^{2+} ($3d^5$) ions because d^5 ions in both high and low spin configurations show many absorption bands. The high-spin Mn^{2+} ions show up to 9 absorption bands related to the spin-forbidden transitions from the $^6A_{1g}(S)$ ground state to excited crystal field states with a multiplicity of 4. The low-spin Mn^{2+} ions show many intense absorption bands related to the spin-allowed transitions from the $^2T_{2g}(I)$ ground state to excited crystal field states with a multiplicity of 2. The observed single absorption band cannot originate from Mn^{4+} ($3d^3$) ions because the Mn^{4+} ions show three

intense optical absorption bands related to the $^4A_{2g}(F) \rightarrow {}^4T_{2g}(F)$, $^4A_{2g}(F) \rightarrow {}^4T_{1g}(F)$, and $^4A_{2g}(F) \rightarrow {}^4T_{1g}(P)$ spin-allowed transitions. The observed absorption band cannot also originate from Mn^{3+} ions in the low-spin configuration. The low-spin Mn^{3+} ions show many intense absorption bands related to spin-allowed transitions from the $^3T_{1g}(H)$ ground state to excited crystal field states with a multiplicity of 3.

It should be noted that a broad absorption band of Mn^{3+} ions with a maximum near 470 nm has been observed in lithium borate glass [39], lithium lead borate glass [14], and aluminum lead borate glass [29]. The position of the Mn^{3+} absorption band in the $Li_2B_4O_7$:Mn, Er glass shows a good correlation with the abovementioned references [14,29,39].

A geometric distortion of the octahedral crystal field (O_h group) with the formation of the elongated or shortened octahedra (D_{4h} group) is very often observed in the glass network. As a result, the ^5E_g state splits into the $^5B_{1g}$ and $^5A_{1g}$ levels, while the $^5T_{2g}$ state splits into the $^5B_{2g}$ and ^5E_g levels. The asymmetric shape of the Mn^{3+} absorption band in the $Li_2B_4O_7$:Mn, Er glass can be related to the superposition of three transitions corresponding to the elongated or shortened octahedron. Used by us, spectroscopic techniques do not provide definitive information regarding the prevailing distortion (elongation or shortening) of the oxygen octahedra in $Li_2B_4O_7$:Mn, Er glass.

The optical absorption spectrum of the $Li_2B_4O_7$:Mn, Er glass also shows several narrow bands peaking at 363 nm, 378 nm, 452 nm, 486 nm, 520 nm, 650 nm, 795 nm, and 974 nm (see inset in Fig. 5). These bands correspond to Er^{3+} ions ($4f^6$ electron configuration) and belong to the $^4I_{15/2} \rightarrow {}^4G_{9/2}$, $^4I_{15/2} \rightarrow {}^4G_{11/2}$, $^4I_{15/2} \rightarrow {}^4F_{5/2}$, $^4I_{15/2} \rightarrow {}^4F_{7/2}$, $^4I_{15/2} \rightarrow {}^2H_{11/2}$, $^4I_{15/2} \rightarrow {}^4F_{9/2}$, $^4I_{15/2} \rightarrow {}^4I_{9/2}$, and $^4I_{15/2} \rightarrow {}^4I_{11/2}$ transitions, respectively. The observed Er^{3+} absorption bands overlap with the broad absorption of the Mn^{3+} ions. Thus, the manganese co-doping causes an increasing and broadening of the absorption of the $Li_2B_4O_7$:Mn, Er glass in comparison with the $Li_2B_4O_7$:Er glass [12] that can be useful to improve the excitation efficiency of the narrow $4f$ – $4f$ transitions of Er^{3+} ions. Luminescence techniques were used to investigate the possibility of $Mn^{3+} \rightarrow Er^{3+}$ energy transfer (see *Subsections 3.4 – 3.5*).

3.4. Luminescence emission and excitation spectra of the $Li_2B_4O_7$:Mn, Er glass

The luminescence emission spectrum of the $Li_2B_4O_7$:Mn, Er glass recorded upon excitation at 411 nm is shown in Fig. 6. It can be seen a broad band extending from 500 nm to 800 nm with a maximum at 618 nm. In our opinion, the observed band belongs to the $^4T_{1g}(G) \rightarrow {}^6A_{1g}(S)$ transition of Mn^{2+} ($3d^5$) ions. The position of the emission maximum at 618 nm indicates an octahedral environment of Mn^{2+} ions in the $Li_2B_4O_7$:Mn, Er glass because Mn^{2+} ions in the octahedral crystal field show the emission maximum in the red spectral range, whereas Mn^{2+} ions in the tetrahedral crystal field show the emission maximum in the green spectral range [40,41]. It should be noted that two deeps are also observed in the luminescence emission spectrum (Fig. 6). A strong deep at 650 nm is related to the $^4I_{15/2} \rightarrow {}^4F_{9/2}$ transition of Er^{3+} ions, whereas a weak deep at 520 nm belongs to the $^4I_{15/2} \rightarrow {}^2H_{11/2}$ transition of Er^{3+} ions. This means that part of the Mn^{2+} emission is absorbed by the Er^{3+} ions.

Fig. 7 shows the luminescence excitation spectrum of $Li_2B_4O_7$:Mn, Er glass recorded under monitoring of the Mn^{2+} emission at 618 nm. Several bands related to Mn^{2+} ions can be observed. The most intense Mn^{2+} excitation band is positioned around 411 nm and belongs to the $^6A_{1g}(S) \rightarrow {}^4A_{1g},{}^4E_g(G)$ transition.

For a more complete understanding, let us analyze the transitions of Mn^{2+} ions. The $3d^5$ electron configuration in the *LS* coupling scheme produces a total of 16 terms. These include one spin sextet, four spin quartets, and eleven spin doublets. The ground ^6S term transforms into the ^6A1_g state in the octahedral crystal field. Under normal circumstances, the high-spin Mn^{2+} configuration exhibits only transitions from the $^6A_{1g}$ state to excited crystal field states characterized by a multiplicity of 4 because transitions to excited states characterized by a multiplicity of 2 have an almost negligible chance of occurring. In the octahedral crystal field, the ^4G term splits into $^4T_{1g}$, $^4T_{2g}$, and $^4A_{1g}$,^4E_g states, the ^4D term splits into $^4T_{2g}$, and ^4E_g states, the ^4P term transforms into the $^4T_{1g}$ state, and the ^4F term splits into $^4A_{2g}$, $^4T_{1g}$, and $^4T_{2g}$ states.

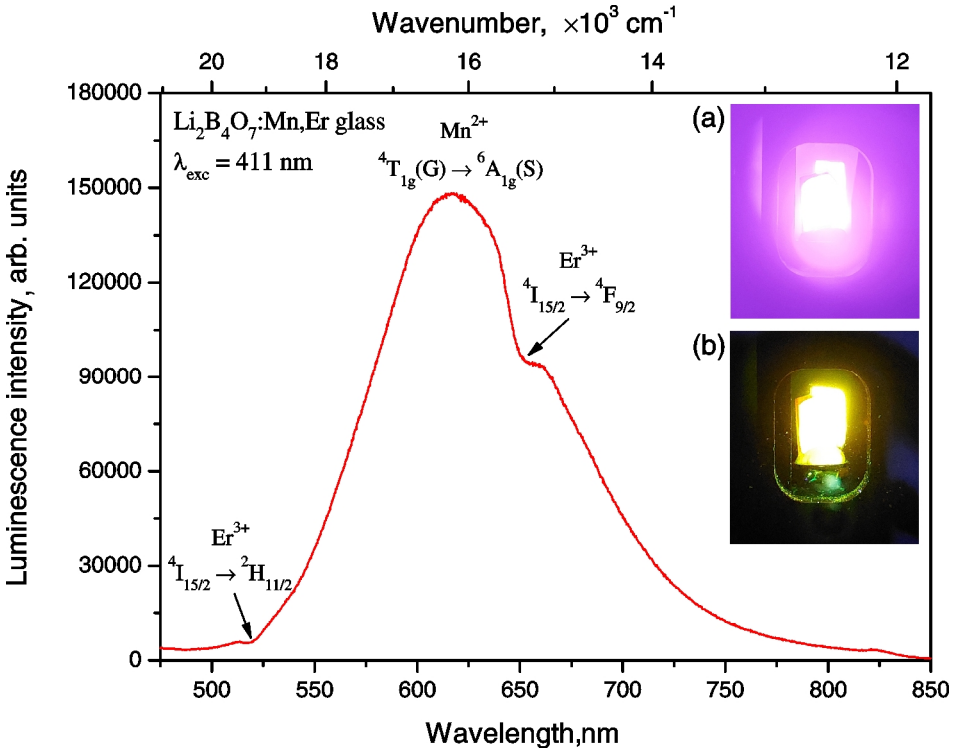

Fig. 6. Luminescence emission spectrum of the $Li_2B_4O_7$:Mn, Er glass recorded upon excitation at λ_{exc} = 411 nm. The luminescent photos of the sample are shown as insets. Photo (a) is made without any optical filters. Photo (b) is made with a 500 nm long pass filter to minimize the violet excitation light on the photo. Photos are made using Samsung A52s smartphone. Focal length of 5.23 mm and aperture of f/1.8 for both photos, ISO of 500 and 3200, and shutter of 1/30 s and 1/4 s for photo (a) and photo (b), respectively.

As mentioned above, several Mn^{2+} bands were observed in the excitation spectrum of the $Li_2B_4O_7$:Mn, Er glass when the red Mn^{2+} emission was monitored. These bands are attributed to Mn^{2+} transitions from the ground $^6A_{1g}$ state to excited crystal field states with a multiplicity of 4 and are denoted in Fig. 7. The optical absorption spectrum lacked Mn^{2+} transitions because the strong and broad Mn^{3+} absorption overshadows the Mn^{2+} spin-forbidden weak absorption bands (see Fig. 5). It should be noted that the correlation between the shape and the approximate wavelength positions of the Mn^{2+} emission and excitation bands in the $Li_2B_4O_7$:Mn, Er glass and those previously reported in [42,43] for different oxide glasses is quite good.

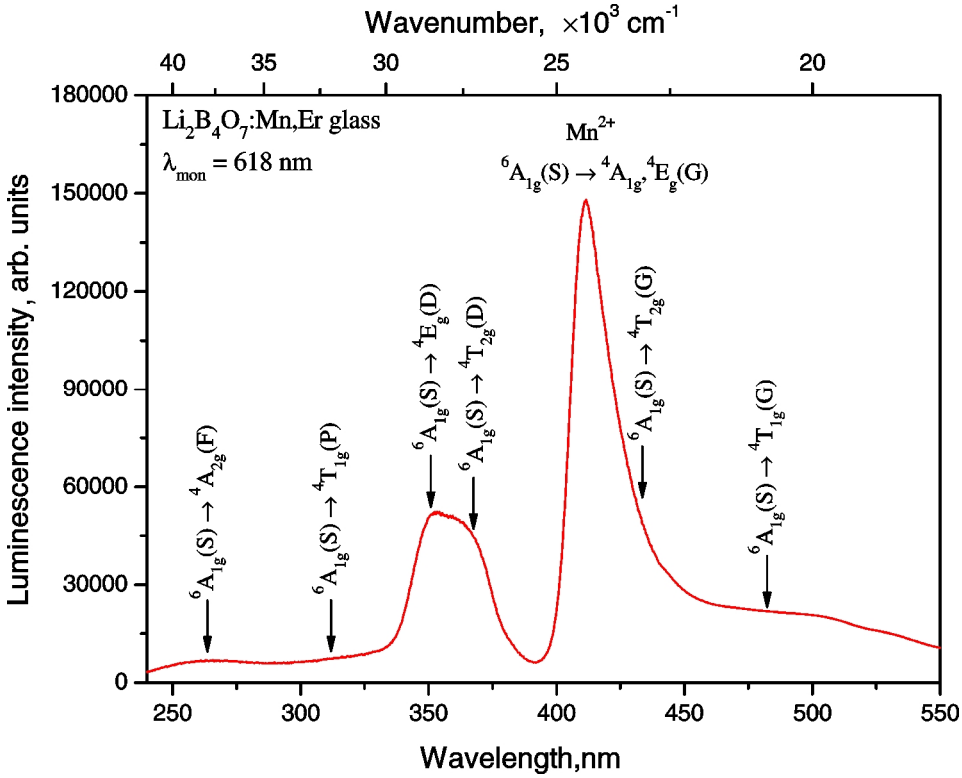

Fig. 7. The luminescence excitation spectrum of the $Li_2B_4O_7$:Mn, Er glass recorded by monitoring of the emission intensity at 618 nm.

The Racah parameters B and C [44] are applied to describe the positions of spectroscopic terms of transition metal ions. Meanwhile, the Tanabe-Sugano diagram [45] is applied to analyze the crystal field splitting. The energy of the $^4A_{1g}$,^4E_g(G), and ^4E_g(D) excited states has no dependence on the crystal field strength (Dq) and, therefore, is equal to the energy of the ^{4}G and ^{4}D terms. Thus, it is possible to calculate the B and C parameters for Mn^{2+} ions in the $Li_2B_4O_7$:Mn, Er glass using the following system of equations:

$$E(^6S \rightarrow {}^4G) = 10B + 5C, \quad E(^6S \rightarrow {}^4D) = 17B + 5C\,. \tag{4}$$

The $^6A_{1g}$(S) → $^4A_{1g}$,^4E_g(G) and $^6A_{1g}$(S) → ^4E_g(D) transitions in the $Li_2B_4O_7$:Mn, Er glass are observed at (411.5 ± 1.0) nm and (351.0 ± 2.0) nm, respectively. Solving the system of equations (4) gives B = (598 ± 25) cm^{-1}, C = (3663 ± 55) cm^{-1}, and C/B = (6.12 ± 0.27). The next step is to build the Tanabe-Sugano diagram at the obtained C/B ratio and to find the Dq/B value which gives the best agreement between the observed and calculated wavelengths of the Mn^{2+} transitions. The Tanabe-Sugano diagram for Mn^{2+} ions in the $Li_2B_4O_7$:Mn, Er glass is shown in Fig. 8.

In this work, the $^6A_{1g}$(S) → $^4T_{2g}$(D) transition at (366.0 ± 2.0) nm was used to calculate the Dq/B value because the maxima of the $^6A_{1g}$(S) → $^4T_{1g}$(G), $^6A_{1g}$(S) → $^4T_{2g}$(G), and $^6A_{1g}$(S) → $^4T_{1g}$(P) transitions in the excitation spectrum of the $Li_2B_4O_7$:Mn, Er glass are more difficult to determine. Using the Tanabe-Sugano diagram (see Fig. 8) and E/B = 45.66 for the $^6A_{1g}$(S) → $^4T_{2g}$(D) transition, it is possible to obtain a value of Dq/B = (0.956 ± 0.001). The calculated Mn^{2+} wavelengths (λ) and energies (E) at the obtained Dq/B value are presented in Table 2.

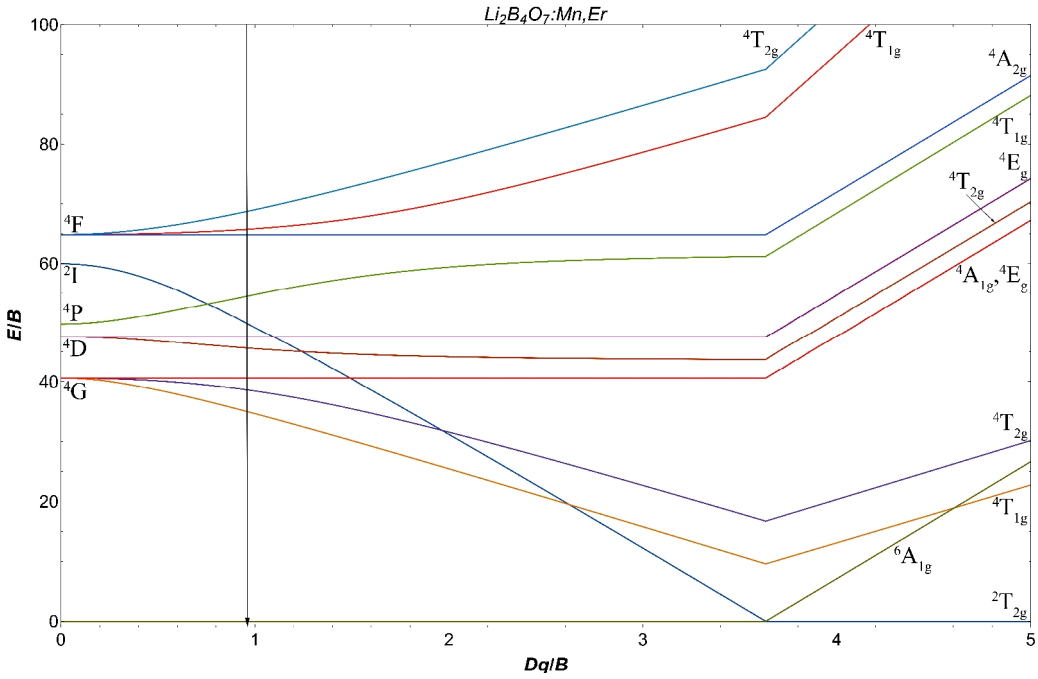

Fig. 8. The Tanabe–Sugano diagram for Mn^{2+} ions in the $Li_2B_4O_7$:Mn, Er glass network.

Based on the obtained values of Dq/B and B, the crystal field strength for Mn^{2+} ions in the $Li_2B_4O_7$:Mn, Er glass was obtained, which equals Dq = (572 ± 24) cm^{-1}. It should be noted that obtained Racah parameters and crystal field strength correlate with literature data for other borate glasses. In particular, the obtained results quite well agree with values B = (633 ± 15) cm^{-1}, C = (3610 ± 15) cm^{-1}, C/B = (5.7 ± 0.1), and Dq = (650 ± 50) cm^{-1}, which were reported in [46] for Mn^{2+} ions in sodium borosilicate glass.

Table 2. The observed and calculated wavelengths (λ) and energies (E) of Mn^{2+} transitions in the $Li_2B_4O_7$:Mn, Er glass. The uncertainty of indirect measurements was calculated using uncertainty propagation.

Transition	Observed		Calculated		
	λ ± 1.0, nm	E, cm^{-1}	E/B ± 0.01	E, cm^{-1}	λ, nm
$^6A_{1g}$ (S) → $^4T_{2g}$ (F)	–		68.70	41110 ± 1700	243 ± 10
$^6A_{1g}$ (S) → $^4T_{1g}$ (F)	–		65.73	39330 ± 1620	254 ± 10
$^6A_{1g}$ (S) → $^4A_{2g}$ (F)	266.0 ± 2.0	37590 ± 280	64.84	38800 ± 1600	258 ± 11
$^6A_{1g}$ (S) → $^4T_{1g}$ (P)	difficult to determine		54.50	32610 ± 1340	307 ± 13
$^6A_{1g}$ (S) → ^4E_g (D)	351.0 ± 2.0	28490 ± 160	47.60	28480 ± 1170	351 ± 14
$^6A_{1g}$ (S) → $^4T_{2g}$ (D)	366.0 ± 2.0	27320 ± 150	45.66	27320 ± 1130	366 ± 15
$^6A_{1g}$ (S) → $^4A_{1g}$,^4E_g (G)	411.5 ± 1.0	24301 ± 59	40.60	24300 ± 1000	412 ± 17
$^6A_{1g}$ (S) → $^4T_{2g}$ (G)	difficult to determine		38.67	23140 ± 950	432 ± 18
$^6A_{1g}$ (S) → $^4T_{1g}$ (G)	difficult to determine		35.04	20970 ± 860	477 ± 20

Luminescence emission and excitation spectra of the $Li_2B_4O_7$:Mn, Er glass registered at excitation and monitoring wavelengths of 316 nm and 370 nm, respectively, are shown in Fig. 9. These spectra focus on the registration of intrinsic luminescence, which has been studied in detail by us for un-doped borate glasses in [47]. The $Li_2B_4O_7$:Mn, Er glass shows an emission band of intrinsic luminescence at 370 nm (see Fig. 9). The corresponding excitation band of intrinsic luminescence peaks at 316 nm (see Fig. 9).

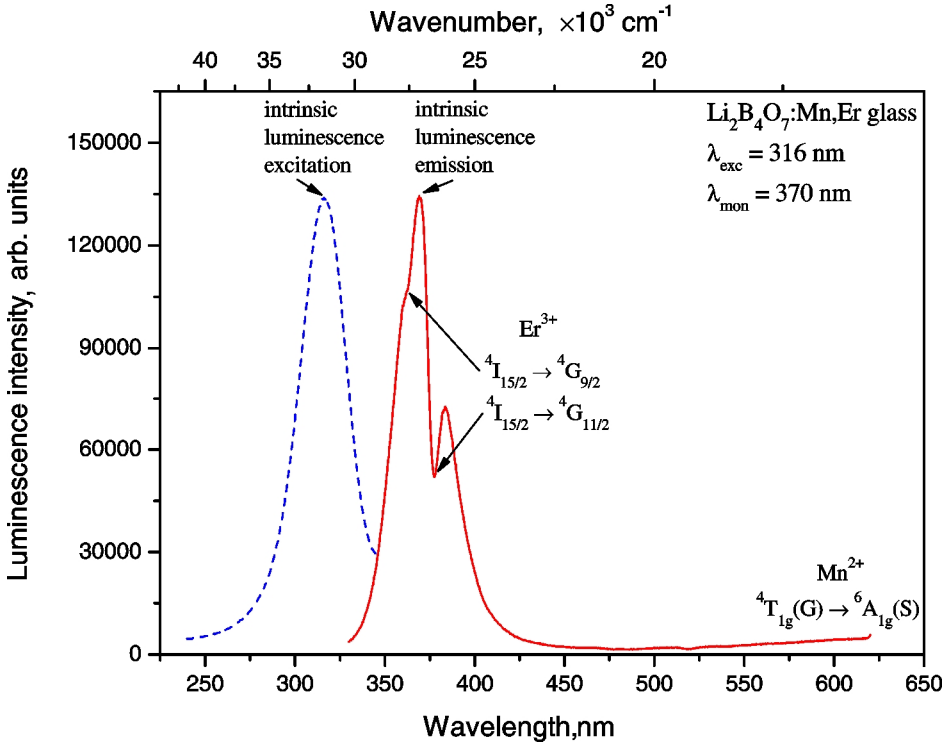

Fig. 9. Luminescence emission (red solid curve) and excitation (blue dashed curve) spectra of the $Li_2B_4O_7$:Mn, Er glass registered at λ_{exc} = 316 nm and λ_{mon} = 370 nm, respectively.

The observed excitation and emission bands are due to band-to-band electronic transitions. Considering the interpretation of the absorption edge (see *Subsection 3.3*), the observed intrinsic luminescence can be related not only to simple electron-hole recombination but also to the creation and annihilation of bound excitons. There are two deeps on the emission band (see Fig. 9). The weaker deep at 363 nm and the stronger deep at 378 nm correspond to the $^4I_{15/2} \rightarrow {}^4G_{9/2}$ and $^4I_{15/2} \rightarrow {}^4G_{11/2}$ transitions of Er^{3+} ions, respectively. This means that part of the intrinsic luminescence is absorbed by Er^{3+} ions. It should be noted that characteristic green luminescence of Er^{3+} ions is not observed in the emission spectrum of the $Li_2B_4O_7$:Mn, Er glass (see Fig. 9). It can be explained by non-radiative processes in Er^{3+} ions and/or energy transfer from Er^{3+} to Mn^{2+} ions. The red Mn^{2+} luminescence is observed upon excitation at 316 nm (see Fig. 9). In this case, Mn^{2+} ions can be directly excited at wavelength 316 nm because the $^6A_{1g}$ (S) → $^4T_{1g}$ (P) transition is close to this wavelength (see Fig. 7). The contribution of energy transfer from the glass network and/or Er^{3+} ions to Mn^{2+} ions also cannot be excluded.

Let us return for a moment to the Mn^{3+} ions, which show the intense broad absorption in the investigated glass (see Fig. 5). Unfortunately, all attempts to register the Mn^{3+}

luminescence were unsuccessful. The Mn^{3+} ions in the $Li_2B_4O_7$:Mn, Er glass exhibit non-radiative transitions to the ground state and do not show any photoluminescence.

3.5. Decay kinetics of the Mn^{2+} luminescence in the $Li_2B_4O_7$:Mn, Er glass

The Mn^{2+} luminescence decay curve in the ions in the $Li_2B_4O_7$:Mn, Er glass is shown in Fig. 10. The decay curve is strongly non-single exponential and can be related to the energy transfer process. The obtained decay kinetics curve of Mn^{2+} ions was fitted quite well by a two-exponential function with lifetime values of τ_1 = 2.62 ms and τ_2 = 10.14 ms (see Fig. 10). The value of the average amplitude lifetime (τ_{avg}) was evaluated according to the following expression:

$$\tau_{avg} = \frac{A_1\tau_1 + A_2\tau_2}{A_1 + A_2}\ , \tag{5}$$

where A_i are amplitudes of lifetimes τ_i (i = 1,2). The calculated amplitude average lifetime of the Mn^{2+} luminescence equals 7.18 ms. For the spin-forbidden $^4T_{1g}(G) \rightarrow {}^6A_{1g}(S)$ transition of the Mn^{2+} ions, a rather long lifetime is typical. For comparison, a lifetime of 5.3 ms was obtained for the $Li_2B_4O_7$:Mn glass in [48]. Thus, a prolonged Mn^{2+} luminescence lifetime is noticed in the $Li_2B_4O_7$:Mn, Er glass compared to the corresponding lifetime in the $Li_2B_4O_7$:Mn glass obtained in [48].

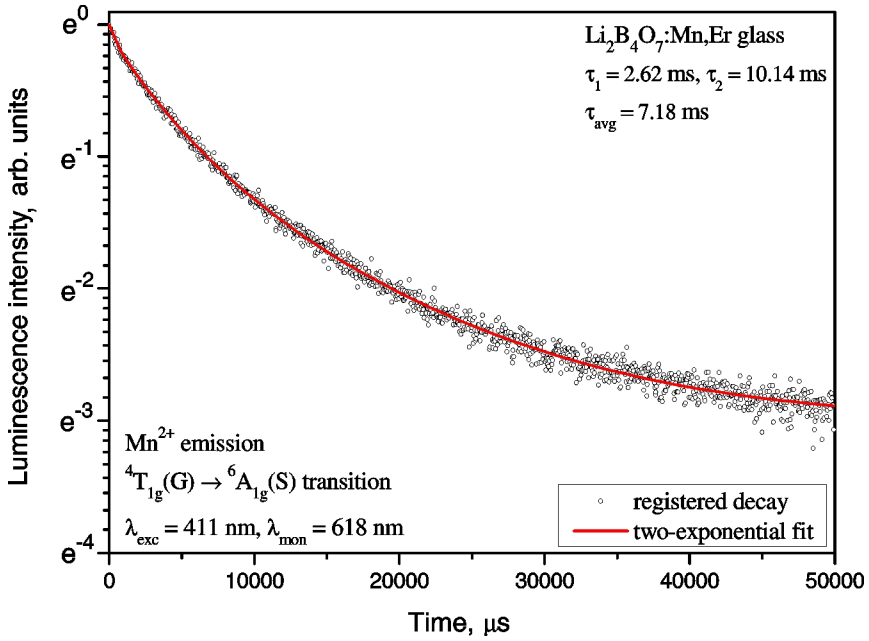

Fig. 10. Luminescence decay kinetics of Mn^{2+} ions in the $Li_2B_4O_7$:Mn, Er glass.

In our opinion, a lifetime extension of the Mn^{2+} luminescence is caused by the $Er^{3+} \rightarrow Mn^{2+}$ energy transfer. The absence (total quenching) of the green Er^{3+} luminescence in the $Li_2B_4O_7$:Mn glass can also be related to the transfer of excitation energy from Er^{3+} to Mn^{2+} ions with subsequent emission of Mn^{2+} ions in the red spectral range. This is the first energy transfer channel in the $Li_2B_4O_7$:Mn, Er glass. The energy of many Er^{3+} transitions overlaps with the broad absorption of Mn^{3+} ions. This fact suggests the possibility of energy transfer from Er^{3+} ions to Mn^{3+} ions followed by non-radiative relaxation to the ground state of the Mn^{3+} ions. This is the second energy transfer channel in the $Li_2B_4O_7$:Mn,Er glass. However, a

detailed analysis of the $Er^{3+} \rightarrow Mn^{3+}$ energy transfer is complicated by the absence of corresponding Er^{3+} emission in the $Li_2B_4O_7$:Mn,Er glass. Proposed possible energy transfer channels ($Er^{3+} \rightarrow Mn^{2+}$, $Er^{3+} \rightarrow Mn^{3+}$) are shown schematically in Fig. 11.

The $Mn^{2+} \rightarrow Mn^{3+}$ energy transfer channel is also possible because the broad absorption of Mn^{3+} ions is extended to the red spectral range, where the Mn^{2+} luminescence is observed. But, in our opinion, such an energy transfer channel is very weak in the $Li_2B_4O_7$:Mn, Er glass. If the $Mn^{2+} \rightarrow Mn^{3+}$ energy transfer was strong enough, then a reduction in the Mn^{2+} lifetime would be expected. This does not occur and the Mn^{2+} ions in the $Li_2B_4O_7$:Mn, Er glass show a longer luminescence lifetime in comparison with the Mn^{2+} lifetime in the $Li_2B_4O_7$:Mn glass.

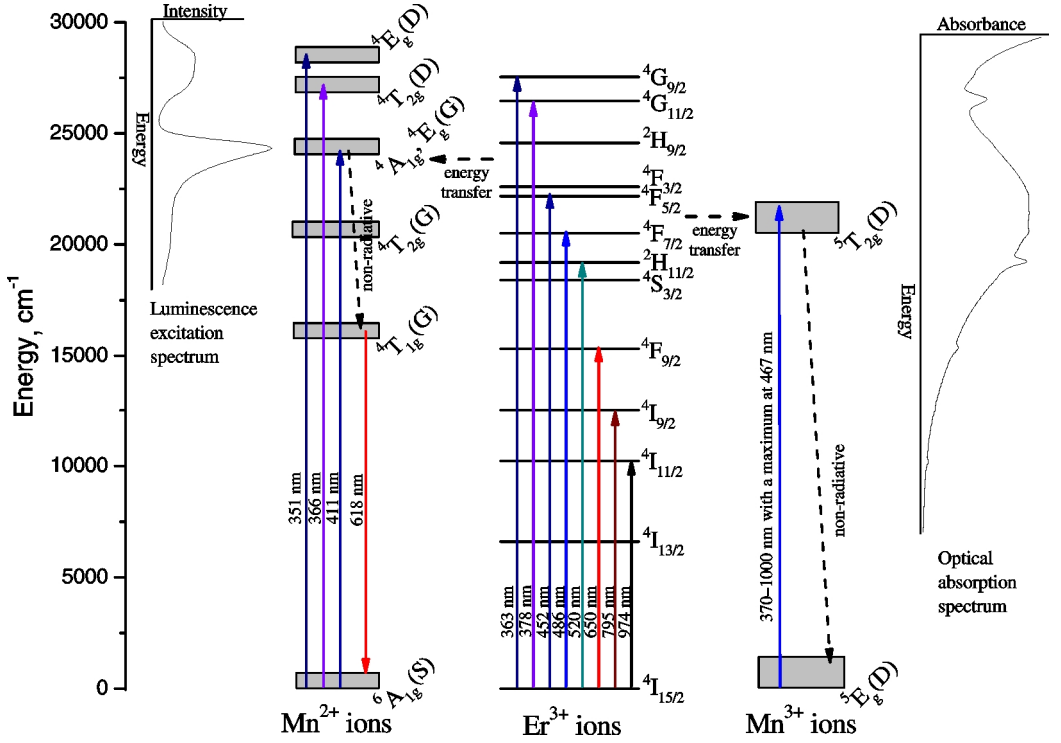

Fig. 11. Partial diagram of Mn^{2+}, Er^{3+}, and Mn^{3+} energy levels in the $Li_2B_4O_7$:Mn, Er glass showing excitation, emission, and energy transfer channels.

4. Conclusions

The XRD, EPR, and optical-luminescent studies of the $Li_2B_4O_7$:Mn, Er glass containing 1.0 mol.% MnO_2 and Er_2O_3 were carefully analyzed, resulting in the following summary.

- The local structure parameters (interatomic distances and coordination numbers) for the $Li_2B_4O_7$:Mn, Er glass, which were derived from the RDF analysis, are similar to corresponding parameters for other co-doped borate glasses with the $Li_2B_4O_7$ basic composition.
- The EPR spectra of the Mn^{2+}, Er^{3+}, and Fe^{3+} ions in the $Li_2B_4O_7$:Mn,Er glass at room and liquid helium temperatures clearly were clearly registered, and their parameters were determined and analyzed in comparison with the EPR data for other glasses.
- In the optical absorption spectrum of the $Li_2B_4O_7$:Mn, Er glass are observed a broad band with a peak at 467 nm that is assigned to the $^5E_g(D) \rightarrow {}^5T_{2g}(D)$ transition of Mn^{3+} ions and narrow bands with peaks at 363, 378, 452, 486, 520, 650, 795, and 974 nm, which

attributed to the transitions from the $^4I_{15/2}$ ground state to the $^4G_{9/2}$, $^4G_{11/2}$, $^4F_{5/2}$, $^4F_{7/2}$, $^2H_{11/2}$, $^4F_{9/2}$, $^4I_{9/2}$, and $^4I_{11/2}$ excited states of the Er^{3+} ions.

- In the luminescence emission spectrum of the $Li_2B_4O_7$:Mn, Er glass was observed a broadband with a peak at 618 nm that assigned to the $^4T_{1g}(G) \rightarrow {}^6A_{1g}(S)$ transition of Mn^{2+} ions. In the luminescence excitation spectrum of the $Li_2B_4O_7$:Mn, Er glass, several bands are observed attributed to the 3d – 3d transitions of Mn^{2+} ions.
- The crystal field splitting analysis for Mn^{2+} ions in the $Li_2B_4O_7$:Mn, Er glass network gave the following values: the Racah parameters B = (598 ± 25) cm^{-1} and C = (3663 ± 55) cm^{-1}, crystal field strength Dq = (572 ± 24) cm^{-1}.
- The average luminescence lifetime of Mn^{2+} ions in the $Li_2B_4O_7$:Mn, Er glass is 7.18 ms, which is slightly longer than the corresponding lifetime value obtained for the $Li_2B_4O_7$:Mn glass.
- The mechanism of excitation energy transfer from Er^{3+} to Mn^{2+} and Mn^{3+} ions in the $Li_2B_4O_7$:Mn, Er glass, which explains the absence of the Er^{3+} and Mn^{3+} luminescence, has been proposed and discussed.

Acknowledgements

This work has been supported by the Vlokh Institute of Physical Optics (Lviv, Ukraine) in the framework of scientific project No. 0122U001833 of the Ministry of Education and Science of Ukraine. The authors would like to thank M.Sc. I.M. Teslyuk from the Vlokh Institute of Physical Optics for sample preparation and Dr Y.O. Kulyk from the Faculty of Physics at the Ivan Franko National University of Lviv for XRD investigation. The authors also thank Prof. I. Stefaniuk and Dr B. Cieniek from the Institute of Materials Engineering at the University of Rzeszów (Poland) for the registration of EPR spectra at low (6.7 – 100 K) temperatures.

References

1. Blasse, G., Grabmaier, B. C. (1994). *Luminescent materials*. Springer Verlag.
2. Shionoya, S., Yen, W. M., & Yamamoto, H. (Eds.). (2007). *Phosphor handbook*. CRC press.
3. Miniscalco, W. J. (1991). Erbium-doped glasses for fiber amplifiers at 1500 nm. *Journal of Lightwave Technology*, *9*(2), 234-250.
4. Mori, A., Ohishi, Y., & Sudo, S. (1997). Erbium-doped tellurite glass fibre laser and amplifier. *Electronics Letters*, *33*(10), 863-864.
5. Jiang, S., Luo, T., Hwang, B. C., Smekatala, F., Seneschal, K., Lucas, J., & Peyghambarian, N. (2000). Er^{3+}-doped phosphate glasses for fiber amplifiers with high gain per unit length. *Journal of Non-Crystalline Solids*, *263*, 364-368.
6. Tanabe, S., Sugimoto, N., Ito, S., & Hanada, T. (2000). Broad-band 1.5 μm emission of Er^{3+} ions in bismuth-based oxide glasses for potential WDM amplifier. *Journal of Luminescence*, *87*, 670-672.
7. Padlyak, B. V., Lisiecki, R., & Ryba-Romanowski, W. (2016). Spectroscopy of the Er-doped lithium tetraborate glasses. *Optical Materials*, *54*, 126-133.
8. Devi, A. R., & Jayasankar, C. K. (1996). Optical properties of Er^{3+} ions in lithium borate glasses and comparative energy level analyses of Er^{3+} ions in various glasses. *Journal of Non-Crystalline Solids*, *197*(2-3), 111-128.
9. Pisarski, W. A., Goryczka, T., Pisarska, J., & Ryba-Romanowski, W. (2007). Er-doped lead borate glasses and transparent glass ceramics for near-infrared luminescence and up-conversion applications. *The Journal of Physical Chemistry B*, *111*(10), 2427-2430.
10. Farouk, M., Samir, A., Metawe, F., & Elokr, M. (2013). Optical absorption and structural studies of bismuth borate glasses containing Er^{3+} ions. *Journal of Non-Crystalline Solids*, *371*, 14-21.
11. Rajagukguk, J., Sinaga, B., & Kaewkhao, J. (2019). Structural and spectroscopic properties of Er^{3+} doped sodium lithium borate glasses. *Spectrochimica Acta Part A: Molecular and Biomolecular Spectroscopy*, *223*, 117342.
12. Kindrat, I. I., Padlyak, B. V., Lisiecki, R., Adamiv, V. T., & Teslyuk, I. M. (2018). Enhancement of the Er^{3+} luminescence in Er–Ag co-doped $Li_2B_4O_7$ glasses. *Optical Materials*, *85*, 238-245.
13. Machado, I. E. C., Prado, L., Gomes, L., Prison, J. M., & Martinelli, J. R. (2004). Optical properties of manganese in barium phosphate glasses. *Journal of Non-Crystalline Solids*, *348*, 113-117.

14. Chakradhar, R. S., Sivaramaiah, G., Rao, J. L., & Gopal, N. O. (2005). EPR and optical investigations of manganese ions in alkali lead tetraborate glasses. *Spectrochimica Acta Part A: Molecular and Biomolecular Spectroscopy*, *62*(4-5), 761-768.
15. Padlyak, B., Vlokh, O., Kukliński, B., & Sagoo, K. (2006). Spectroscopy of Mn-doped glasses of $CaO\text{-}Ga_2O_3\text{-}GeO_2$ system. *Ukrainian Journal of Physical Optics*, *7*(1), 1-10.
16. Turnbull, D. A., & Bishop, S. G. (1997). Effect of transition metal co-doping on broad band luminescence excitation mechanism in rare earth-doped chalcogenide glasses. *Journal of Non-Crystalline Solids*, *213*, 288-294.
17. De Herval, L. K. S., Arslanlar, Y. T., Ayvacikli, M., Iikawa, F., Nobrega, J. A., Pizani, P. S., Gobato, Y. G., Can, N., Henini, M. & De Godoy, M. P. F. (2015). Enhancement of the luminescence intensity by co-doping Mn^{2+} into Er^{3+}-doped $SrAl_2O_4$. *Journal of Luminescence*, *163*, 17-20.
18. Liao, J., Wang, M., Han, Z., Huang, J., Gong, G., Fu, J., & Wen, H. R. (2021). Luminescence properties and energy transfer mechanism of $La_2ZnTiO_6:Mn^{4+}/Er^{3+}$ far-red/green dual-emitting phosphors for plant lighting. *Journal of Solid State Chemistry*, *303*, 122470.
19. Zhang, X., Zhao, J., Chen, B., Sun, T., Ma, R., Wang, Y., Zhu, H., Peng, D. & Wang, F. (2020). Tuning multimode luminescence in lanthanide (III) and manganese (II) co-doped CaZnOS crystals. *Advanced Optical Materials*, *8*(11), 2000274.
20. Song, P., Hase, S., Zhao, S., Xu, Z., Iso, Y., & Isobe, T. (2022). Feasibility of emission-enhanced $CsPbCl_3$ quantum dots co-doped with Mn^{2+} and Er^{3+} as luminescent downshifting layers in crystalline silicon solar modules. *ACS Applied Nano Materials*, *5*(2), 2522-2531.
21. Padlyak, B. V., Drzewiecki, A., & Smyrnov, O. O. (2010). EPR spectroscopy of tetraborate glasses, doped with Mn and Cu. *Current Topics in Biophysics*, *33*(Suppl A), 171-175.
22. Padlyak, B. V., Mudry, S. I., Kulyk, Y. O., Drzewiecki, A., Adamiv, V. T., Burak, Y. V., & Teslyuk, I. M. (2012). Synthesis and X-ray structural investigation of undoped borate glasses. *Materials Science-Poland*, *30*, 264-273.
23. Krogh-Moe, J. (1968). Refinement of the crystal structure of lithium diborate $Li_2O.2B_2O_3$. *Acta Crystallographica Section B: Structural Crystallography and Crystal Chemistry*, *24*(2), 179-181.
24. Antao, S. M., Hassan, I., Wang, J., Lee, P. L., & Toby, B. H. (2008). State-of-the-art high-resolution powder X-ray diffraction (HRPXRD) illustrated with Rietveld structure refinement of quartz, sodalite, tremolite, and meionite. *The Canadian Mineralogist*, *46*(6), 1501-1509.
25. Padlyak, B. V., Kindrat, I. I., Adamiv, V. T., Drzewiecki, A., & Stefaniuk, I. (2024). Spectroscopic properties and photoluminescence of the $Li_2B_4O_7$:Mn,Sm glass. *Materials Research Bulletin*, *175*, 112788.
26. Griscom, D. L. (1980). Electron spin resonance in glasses. *Journal of Non-Crystalline Solids*, *40*(1-3), 211-272.
27. Brodbeck, C. M., & Bukrey, R. R. (1981). Model calculations for the coordination of Fe^{3+} and Mn^{2+} ions in oxide glasses. *Physical Review B*, *24*(5), 2334.
28. Padlyak, B. V., & Gutsze, A. (1998). EPR study of the impurity paramagnetic centres in ($CaO\text{-}Ga_2O_3\text{-}GeO_2$) glasses. *Applied Magnetic Resonance*, *14*, 59-68.
29. Sivaramaiah, G., & LakshmanaRao, J. (2012). Electron spin resonance and optical absorption spectroscopic studies of manganese centers in aluminium lead borate glasses. *Spectrochimica Acta Part A: Molecular and Biomolecular Spectroscopy*, *98*, 105-109.
30. Iton, L. E., & Turkevich, J. (1977). Electron paramagnetic resonance of rare earth ions in zeolites. *The Journal of Physical Chemistry*, *81*(5), 435-449.
31. Antuzevics, A. (2020). EPR characterization of erbium in glasses and glass ceramics. *Low Temperature Physics*, *46*(12), 1149-1153.
32. Yamada, H., & Kojima, K. (1999). Upconversion fluorescence in Er^{3+}-doped $Na_2O–GeO_2$ glasses. *Journal of Non-Crystalline Solids*, *259*(1-3), 57-62.
33. Kaewwiset, W., Thamaphat, K., Kaewkhao, J., & Limsuwan, P. (2013). ESR and spectral studies of Er^{3+} ions in soda-lime silicate glass. *Physica B: Condensed Matter*, *409*, 24-29.
34. Castner Jr, T., Newell, G. S., Holton, W. C., & Slichter, C. P. (1960). Note on the paramagnetic resonance of iron in glass. *The Journal of Chemical Physics*, *32*(3), 668-673.
35. Padlyak, B. V., & Padlyak, T. B. (2020). Spectroscopic properties of the V-doped borate glasses. *Journal of Non-Crystalline Solids*, *528*, 119741.
36. Padlyak, B. V., Kindrat, I. I., Drzewiecki, A., Goleus, V. I., & Hordieiev, Y. S. (2021). Spectroscopic properties and intrinsic photoluminescence of the un-doped lead borate glasses. *Journal of Non-Crystalline Solids*, *557*, 120631.
37. Padlyak, B. V., Kindrat, I. I., Kulyk, Y. O., Hordieiev, Y. S., Goleus, V. I., & Lisiecki, R. (2023). Structural features and optical-luminescent properties of the Pb-containing germanate and silicate oxyfluoride glasses. *Materials Science and Engineering: B*, *293*, 116460.

38. Rukang, L. I. (1989). The interpretation of UV absorption of borate glasses and crystals. *Journal of Non-Crystalline Solids*, *111*(2-3), 199-204.
39. Terczyńska-Madej, A., Cholewa-Kowalska, K., & Łączka, M. (2011). Coordination and valence state of transition metal ions in alkali-borate glasses. *Optical Materials*, *33*(12), 1984-1988.
40. Satyanarayana, T., Valente, M. A., Nagarjuna, G., & Veeraiah, N. (2013). Spectroscopic features of manganese doped tellurite borate glass ceramics. *Journal of Physics and Chemistry of Solids*, *74*(2), 229-235.
41. Lewandowski, T., Łapiński, M., Walas, M., Prześniak-Welenc, M., & Wicikowski, L. (2017). Role of MnO in manganese–borate binary glass systems: a study on structure and thermal properties. *Bulletin of Materials Science*, *40*, 933-938.
42. Wen, H., Tanner, P. A., & Cheng, B. M. (2016). Optical properties of $3d^N$ transition metal ion-doped lead borate glasses. *Materials Research Bulletin*, *83*, 400-407.
43. Othman, H., Elkholy, H., Cicconi, M. R., Palles, D., de Ligny, D., Kamitsos, E. I., & Möncke, D. (2020). Spectroscopic study of the role of alkaline earth oxides in mixed borate glasses - site basicity, polarizability and glass structure. *Journal of Non-Crystalline Solids*, *533*, 119892.
44. Racah, G. (1942). Theory of complex spectra. II. *Physical Review*, *62*(9-10), 438.
45. Tanabe, Y., & Sugano, S. (1954). On the absorption spectra of complex ions I. *Journal of the Physical Society of Japan*, *9*(5), 753-766.
46. Menassa, P. E., Simkin, D. J., & Taylor, P. (1986). Spectroscopic investigations of Mn^{2+} in sodium borosilicate glasses. *Journal of Luminescence*, *35*(4), 223-233.
47. Kindrat, I. I., Padlyak, B. V., & Drzewiecki, A. (2017). Intrinsic luminescence of un-doped borate glasses. *Journal of Luminescence*, *187*, 546-554.
48. Drzewiecki, A. (2016). *Structure and spectroscopic properties of borate glasses, doped with iron-group elements*, PhD thesis, University of Zielona Góra.

B.V. Padlyak, I.I. Kindrat, A. Drzewiecki, V.T. Adamiv. (2024). Spectroscopic and Optical-Luminescent Properties of the $Li_2B_4O_7$:Mn, Er Glass**.** *Ukrainian Journal of Physical Optics*, *25*(3), 03105 – 03124. doi: 10.3116/16091833/Ukr.J.Phys.Opt.2024.03105

Анотація*. Високоякісні зразки скла $Li_2B_4O_7$:Mn,Er, що містять 1,0 мол.% MnO_2 та Er_2O_3, вперше отримані за технологією охолодження розплаву та досліджені методами рентгенівської дифракції (XRD), електронного парамагнітного резонансу (ЕПР) та оптико-люмінесцентної спектроскопії. З функції радіального розподілу, розрахованої з експериментальної кривої XRD, були отримані параметри локальної структури (міжатомні відстані та координаційні числа) скла $Li_2B_4O_7$:Mn,Er. На основі аналізу даних ЕПР та оптичної спектроскопії (поглинання, збудження люмінесценції, люмінесценція, кінетика загасання) виявлено наявність іонів $Mn^{2+}(3d^5)$, $Mn^{3+}(3d^4)$ та Er^{3+} $(4f^{11})$ у сітці скла $Li_2B_4O_7$:Mn,Er. Зокрема, у досліджуваному склі ідентифіковано три типи центрів Mn^{2+}: поодинокі іони $Mn^{2+}(1)$ у сильно спотворених вузлах ромбічної симетрії (співвідношення ромбічної та осьової констант $|E/D| \leq 1/3$), поодинокі іони $Mn^{2+}(2)$ у вузлах майже кубічної симетрії ($D \cong 0$, $E \cong 0$), а також пари Mn^{2+} і малі кластери, пов'язані між собою магнітною дипольною та обмінною взаємодіями. Спектр оптичного поглинання скла $Li_2B_4O_7$:Mn,Er демонструє дуже широку, інтенсивну смугу з піком при 467 нм, яка належить до переходу $^5E_g(D) \rightarrow {}^5T_{2g}(D)$ іонів Mn^{3+}, і низку слабких, вузьких ліній, що належать f - f переходам іонів Er^{3+} $(4f^{11}, {}^4I_{15/2})$. Спектр люмінесценції скла $Li_2B_4O_7$:Mn,Er демонструє широку смугу, що відповідає переходу $^4T_{1g}(G) \rightarrow {}^6A_{1g}(S)$ іонів Mn^{2+}. Спектри люмінесценції та кінетику загасання центрів Mn^{2+} у склі $Li_2B_4O_7$:Mn,Er обговорено та порівняно з відповідними результатами для скла $Li_2B_4O_7$:Mn. Відсутність характерної фотолюмінесценції Er^{3+} та Mn^{3+} у склі $Li_2B_4O_7$:Mn,Er пояснюється запропонованими механізмами передачі енергії від іонів Er^{3+} до іонів Mn^{2+} та Mn^{3+}.*

Ключові слова*: $Li_2B_4O_7$:Mn, Er скло, XRD, ЕПР, оптичне поглинання, фотолюмінесценція, кінетика загасання, перенесення енергії*